



Obrabotka metallov -

Metal Working and Material Science

Journal homepage: http://journals.nstu.ru/obrabotka_metallov



Structure and properties of HEA-based coating reinforced with CrB particles

Alexey Ruktuev^{1, a, *}, Aleksandr Yurgin^{1, b}, Vladislav Shikalov^{2, c}, Arina Ukhina^{3, d}, Ivan Chakin^{4, e},
 Evgeny Domarov^{4, f}, Gleb Dovzhenko^{5, g}

¹ Novosibirsk State Technical University, 20 Prospekt K. Marksa, Novosibirsk, 630073, Russian Federation

² Khristianovich Institute of Theoretical and Applied Mechanics SB RAS, 4/1 Institutskaya str., Novosibirsk, 630090, Russian Federation

³ Institute of solid state chemistry and mechanochemistry SB RAS, 18 Kutateladze str., Novosibirsk, 630090, Russian Federation

⁴ Budker Institute of nuclear physics SB RAS, 11 Lavrentyeva str., Novosibirsk, 630090, Russian Federation

⁵ SRF "SKIF", 1 Nikolsky Prospekt, Koltsovo, 630559, Russian Federation

^a  <https://orcid.org/0000-0002-1325-1533>,  ruktuev@corp.nstu.ru, ^b  <https://orcid.org/0000-0003-0473-7627>,  yurgin2012@yandex.ru,

^c  <https://orcid.org/0000-0002-0491-2803>,  v.shikalov@gmail.com, ^d  <https://orcid.org/0000-0003-1878-0538>,  auhina181@gmail.com,

^e  <https://orcid.org/0000-0003-0529-2017>,  chak_in2003@bk.ru, ^f  <https://orcid.org/0000-0003-2422-1513>,  domarov88@mail.ru,

^g  <https://orcid.org/0000-0003-0615-0643>,  g.d.dovzhenko@srf-skif.ru

ARTICLE INFO

Article history:

Received: 07 April 2023

Revised: 25 April 2023

Accepted: 11 May 2023

Available online: 15 September 2023

Keywords:

Electron beam surfacing

Chromium boride

CoCrFeNiMn

High entropy alloy

Coating

Funding

This study was funded by Russian Science Foundation No. 22-79-00189, <https://rscf.ru/project/22-79-00189/>.

Acknowledgements

Structural investigations were conducted at core facility "Structure, mechanical and physical properties of materials"; wear resistance test was conducted at core facility "Mechanics".

ABSTRACT

Introduction. Currently, a new class of materials, namely high-entropy alloys, is an active area of research. One of the areas of its application is the fabrication of protective coatings with high performance properties. The high-entropy alloy of *CoCrFeNiMn* composition is characterized by high ductility, which is retained both at elevated and cryogenic temperatures, as well as high thermal stability and, thus, can be considered as promising materials for protective coatings formation. At the same time, its disadvantages are low hardness and strength. It is known that the reinforcement of the *CoCrFeNiMn* high-entropy alloy with hardening particles is an effective way to improve the mechanical properties of coatings. It is assumed that the addition of hardening boride particles affects positively on the mechanical characteristics of the alloy. The **aim of this work** is to study the structural and phase states and wear resistance of coatings based on a *CoCrFeNiMn* high-entropy alloy reinforced with *CrB* particles. Coatings obtained by the method of non-vacuum electron-beam surfacing of powder mixtures with different mass ratios of *CoCrNiMn* metal powders to the *CrB* powder (100:0, 95:5, 90:10, 80:20, 70:30) are studied in this work. To investigate the structure and phase composition of the coatings, such methods as optical microscopy, scanning electron microscopy and X-ray diffraction analysis were applied. To study the elemental composition, energy-dispersive X-ray analysis was used. The mechanical properties were evaluated based on the microhardness measuring results. The wear resistance of the coatings was determined under conditions of dry sliding friction during reciprocating motion. **Results and discussion.** The addition of *CrB* powder to the surfacing mixture led to the formation of eutectic structures. When 5 wt. % *CrB* was added, a hypoeutectic structure is formed in the coating. An increase in the amount of *CrB* leads to the formation of coatings with a hypereutectic structure containing primary borides. The main phases found in the coatings are the *fcc* solid solution, and $(Cr,Mn,Fe)_2B$, $(Ni,Co,Mn)_2B$, *CrB* borides. All the studied coatings are characterized by an adhesive wear mechanism. The addition of 20 % and 30 % *CrB* to the surfacing mixture composition results in the wear resistance increase of the high-entropy alloy-based coatings by 3.6 and 6.1 times, respectively.

For citation: Ruktuev A.A., Yurgin A.B., Shikalov V.S., Ukhina A.V., Chakin I.K., Domarov E.V., Dovzhenko G.D. Structure and properties of HEA-based coating reinforced with CrB particles. *Obrabotka metallov (tehnologiya, oborudovanie, instrumenty) = Metal Working and Material Science*, 2023, vol. 25, no. 3, pp. 87–103. DOI: 10.17212/1994-6309-2023-25.3-87-103. (In Russian).

* Corresponding author

Ruktuev Alexey A., Ph.D. (Engineering), Associate Professor
 Novosibirsk State Technical University,
 20 Prospekt K. Marksa,
 630073, Novosibirsk, Russian Federation
 Tel.: +7 (383) 346-06-12, e-mail: ruktuev@corp.nstu.ru

Introduction

Intensive wear of parts operating under friction conditions, at elevated temperatures, and in aggressive medium is one of the problems in the engineering equipment operation. To ensure long-term service, materials used in such conditions should possess high wear resistance, heat resistance, corrosion resistance, and fracture toughness. Conventionally used materials based on metal alloys, ceramics or intermetallic compounds cannot always provide the required level of performance characteristics. A new approach based on the fusion of several elements with a concentration of each equal to 5–35 at. % has been actively explored in the last 15 years [1, 2]. Due to the high configurational entropy, such materials are called **high-entropy alloys (HEAs)**. This approach leads to an almost limitless number of possible alloy compositions. It was mentioned in studies [3–6] that *HEAs* can demonstrate an outstanding combination of physical and mechanical properties, such as high strength at elevated and cryogenic temperatures, high ductility, good corrosion resistance, and wear resistance. At the same time, it should be noted that the *HEAs* are composed of a large number of expensive elements, which increases the product cost.

An effective solution to the problem of cost combined with performance consists in the formation of protective layers on its surfaces with properties comparing favorably with those of the base material. The abovementioned peculiarities of *HEAs* make these materials promising for the protective coatings formation [7, 8]. Various technologies, such as laser surface coating [9–11], plasma spraying [12, 13], and others [7] can be used to fabricate structural coatings based on high-entropy alloys. In this work, for coating formation, the non-vacuum electron-beam surfacing method [14] was applied, which has previously been successfully used to obtain protective coatings on stainless steels [15, 16], titanium [17], and low-carbon steels [18–20].

The *CoCrFeNiMn* alloy, also known as the *Kantor* alloy, is one of the well-studied *HEAs* [21–26]. This alloy is characterized by high plasticity [27], which is retained both at elevated and cryogenic temperatures, as well as high thermal stability, but low strength characteristics. To improve the mechanical properties of the *CoCrFeMnNi* alloy, various approaches based on cold plastic deformation [28], thermomechanical treatment, optimization of the elemental composition of the alloy [29], and the appending additional elements, such as aluminum or vanadium [30, 31], can be used. Another approach to improving the properties consists in the formation of alloys or coatings with a composite structure formed of a high-entropy matrix reinforced with ceramic particles. At present, *TiC* [9, 10, 32], *SiC* [33], *WC* [34] carbides, as well as oxides and nitrides [35] are used as reinforcing particles in the published works. In the mentioned studies, it was shown that the formation of a composite structure made it possible to improve effectively the strength and tribological properties of high-entropy alloys. Borides are another type of particles that allow increasing the hardness and wear resistance of materials [36, 37]. However, it should be noted that the effect of boron-containing compounds on the structure and properties of high-entropy alloys has not been studied extensively.

The purpose of this work was to study the structure and phase composition of *CoCrFeNiMn*-based *HEA* coatings reinforced with *CrB* particles and to estimate the effect of borides on the wear resistance level of the reinforced layers.

Materials and methods

The specimens with coatings were produced by non-vacuum electron-beam surfacing with the use of an *ELV-6M* industrial electron accelerator at the *Budker Institute of Nuclear Physics, SB RAS*. Steel 20 workpieces with a size of $100 \times 50 \times 10$ mm³ were used as the base material. The coatings were formed from a powder mixture consisting of metal powders (*Co*, *Cr*, *Ni*, *Mn*), chromium boride powder, and flux powder. *CaF₂* was used as a flux to protect the melt pool from interaction with the atmosphere. Commercially pure metal powders were preliminarily mixed by an equiatomic ratio. To obtain a series of experimental specimens, mixtures were prepared with different mass ratios of the *CoCrNiMn* composition of metal powders to a *CrB* powder (100:0, 95:5, 90:10, 80:20, 70:30). The mass ratio of the surfacing powders and the flux was constant (7:3). It should be noted that an iron powder was not added to the mixture composition

because iron inflowed to the coating during the melting of the base material. The compositions of the used powder mixtures are shown in Table 1. The prepared mixtures were put on the surfaces of a steel workpieces with a packed density of 0.8 g/cm^2 .

The main technological modes of surfacing that affect the energy density are presented in Table 2. The workpiece motion speed and the electron beam current were selected in such a way as to provide the equiatomic composition of the *CoCrFeNiMn* coating without *CrB* particles (1st mode). Modes 3, 4, and 5 provided increased electron beam current to compensate for the rise in the melting temperature of the powder mixture.

Table 1

Compositions of surfacing powder mixtures

No.	Surfacing powders, wt. %	Flux, wt. %
1	<i>CoCrNiMn</i> 70%	CaF_2 30%
2	(<i>CoCrNiMn</i> : <i>CrB</i> 95:5) 70%	
3	(<i>CoCrNiMn</i> : <i>CrB</i> 90:10) 70%	
4	(<i>CoCrNiMn</i> : <i>CrB</i> 80:20) 70%	
5	(<i>CoCrNiMn</i> : <i>CrB</i> 70:30) 70%	

Table 2

Technological modes of surfacing

No.	Composition	Beam current, mA	Accelerating voltage, MeV	Workpiece motion speed, cm/s	Energy density, kJ/cm^2
1	<i>CoCrNiMn</i>	25	1.4	1.5	4.67
2	<i>CoCrNiMn</i> : <i>CrB</i> 95:5	25			
3	<i>CoCrNiMn</i> : <i>CrB</i> 90:10	26.5			
4	<i>CoCrNiMn</i> : <i>CrB</i> 80:20	26.5			4.95
5	<i>CoCrNiMn</i> : <i>CrB</i> 70:30	26.5			

The microstructure of the coatings was studied in transverse sections prepared according to the standard method: grinding using abrasive papers with a gradual decrease in grit from *P180* to *P4000* and final polishing using an alumina suspension with a particle size of $0.3 \mu\text{m}$. To reveal the structure, prepared samples were chemically etched with a solution consisting of 10 ml HNO_3 + 10 ml HF + 15 ml H_2O for 10–60 sec. The microstructure was studied using a *Carl Zeiss AxioObserver Z1.m* optical microscope and a *Carl Zeiss EVO50 XVP* scanning electron microscope equipped with an *Oxford Instruments INCA X-Act* system for X-ray energy dispersive microanalysis.

The phase composition of the coatings was studied by a *Bruker D8 ADVANCE* X-ray diffractometer using *Cu K α* radiation. The diffraction patterns were recorded in the range of $2\Theta = 15\text{--}90^\circ$ with a step of 0.02° . The dwell time was 0.2 s per point. The diffraction patterns were analyzed using the *ICDD PDF4+* database.

The microhardness of the coatings was determined by the *Vickers* method with a *WolpertGroup 402 MVD* hardness tester on polished transverse sections. The load on the indenter was 100 g, the dwell time was 15 s.

The wear resistance of the coatings was evaluated under dry reciprocating sliding friction conditions. The ball-on-flat test scheme corresponded to the *ASTM G133-05* standard. Tests were performed using a *Bruker UMT-2* universal friction machine. A ball made of *VK-6 (WC-6Co)* cemented carbides alloy with a diameter of 6.35 mm was used as a counterbody. The coatings were tested under the following parameters: the load on the counterbody was 25 N, the stroke length per cycle was 5 mm, and the total sliding distance was 100 m. Before testing, the specimens were ground and polished according to the sample preparation method for microstructural studies. The volume of worn material was determined using a *Bruker Contour GT-K1* optical profilometer.

Results and discussion

Results of microstructural studies

In the cross sections of the coated samples, several zones typical for the materials obtained by surfacing technologies can be distinguished: the surfaced layer, the heat-affected zone in the base material, and the zone of the base metal unaffected by significant heating. The thickness of the surfaced layers was about 1 mm. Dendritic structure is clearly seen in the structure of all coatings at low magnifications (fig. 1). In the coating obtained without *CrB* appending, the detected dendritic inhomogeneity is associated with the redistribution of elements during crystallization resulting in the enrichment of interdendritic space in manganese and nickel and the deficiency of these elements in the dendrites. However, the structure formed in this case was single-phase. A detailed analysis of the *CoCrFeNiMn* coating structure was performed earlier in [38]. The formation of dendritic inhomogeneity in the coatings obtained with *CrB* appending was accompanied by the precipitation of borides of various morphologies and compositions. It should be noted that in coatings without *CrB* and with 5 % *CrB* (hereinafter, wt. % is used, unless otherwise indicated) (fig. 1a, b), the vertical direction of the formed structure is clearly distinguished, which can be explained by a small number of crystallization centers and a high temperature gradient arising due to the predominant heat flow towards the base material. In the coatings obtained with 10–30 % *CrB* appending (fig. 1c–e), primary

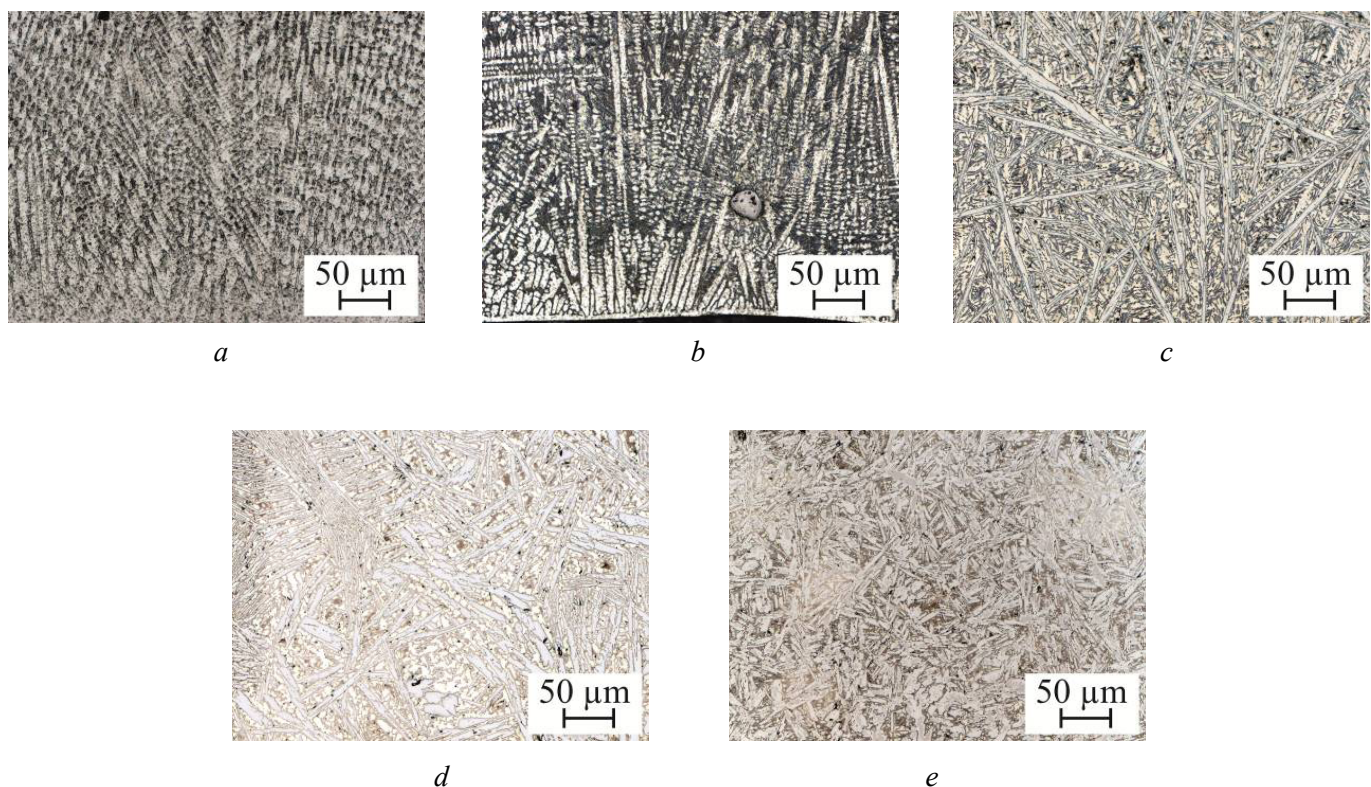


Fig. 1. Microstructure of the specimens obtained by surfacing the powder mixtures with different *CrB* content: a – 0 % *CrB*; b – 5 % *CrB*; c – 10 % *CrB*; d – 20 % *CrB*; e – 30 % *CrB*

borides were revealed in the structure, which presumably prevent the formation of an oriented structure during the crystallization of the melt pool.

Fig. 2 shows the microstructure of the coatings obtained by surfacing the mixtures with 5 % and 10 % *CrB*. The appending of 5 % *CrB* led to the formation of a coating with a hypoeutectic structure represented by a metal matrix and a fine lamellar eutectic located in the interdendritic regions. The structure of the coatings obtained from mixtures containing 10 % *CrB* is hypereutectic. In the coating, primary borides with lamellar eutectic between them were formed (fig. 2b).

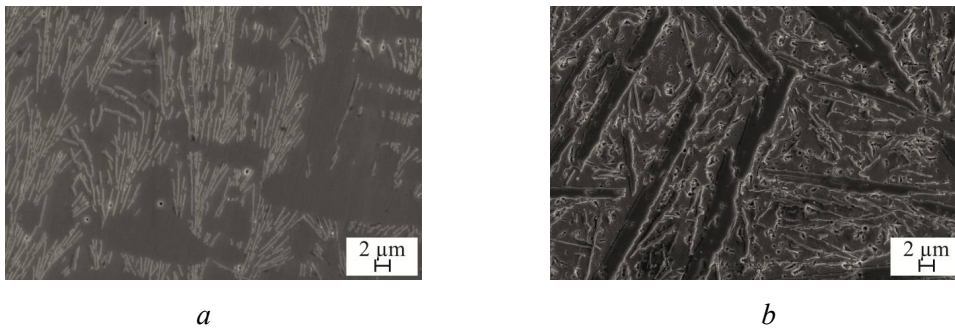


Fig. 2. Microstructure of borides in the coatings obtained by surfacing the powder mixtures with different *CrB* content:

a – 5 % *CrB*; *b* – 10 % *CrB*

Fig. 3 shows the elemental distribution maps from the coating obtained with the appending of 10 % *CrB*. The boron distribution map is not provided because of the low accuracy of the determination of light elements by the energy dispersive analysis. It can be seen in Fig. 3 that the chromium concentration is maximum in the primary boride crystals and eutectic borides and decreases in the metal matrix. Manganese and iron are distributed more evenly and can be found in both the borides and the matrix, while nickel and cobalt are predominantly present in the matrix.

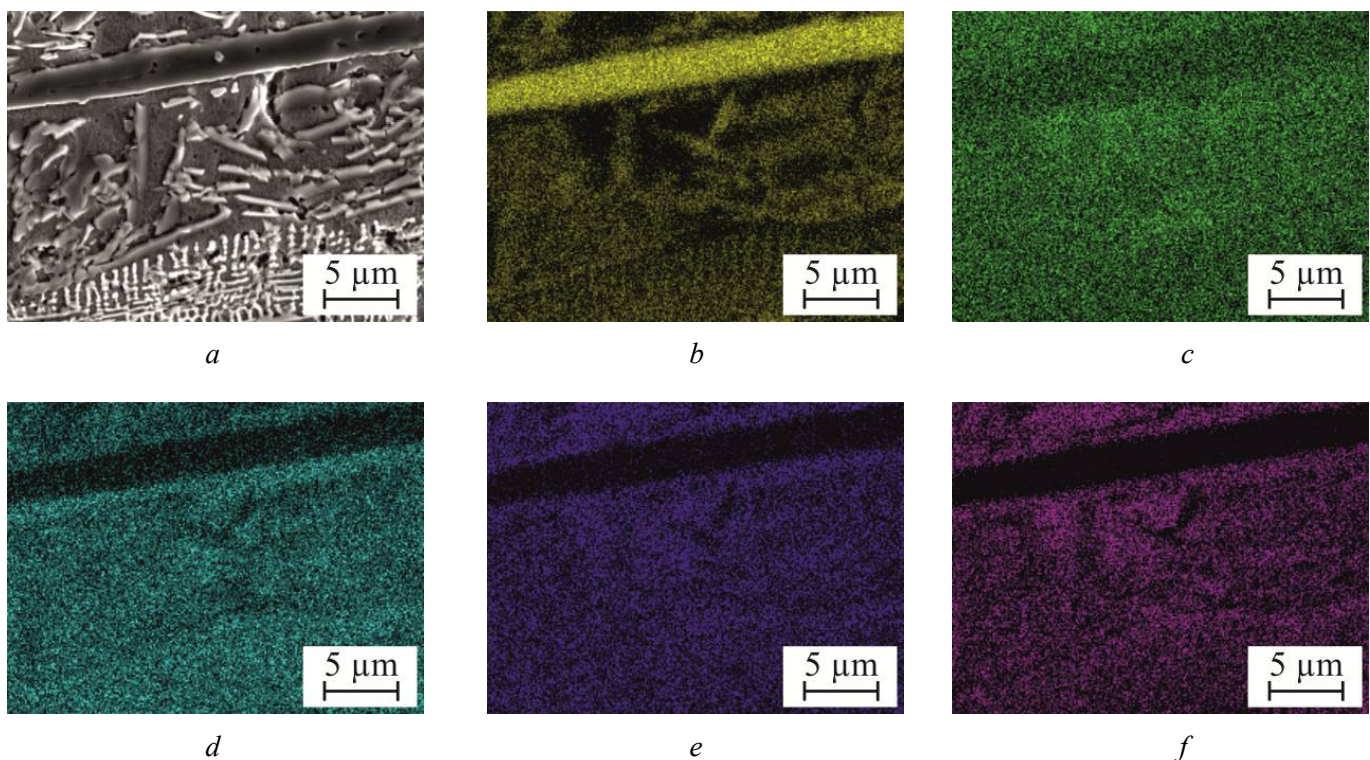


Fig. 3. Distribution of elements in the structure of the coating obtained by surfacing the powder mixture with 10 % *CrB*:

a – microstructure of the analyzed region; *b* – *Cr*; *c* – *Mn*; *d* – *Fe*; *e* – *Co*; *f* – *Ni*

An increase in *CrB* amount in the surfacing mixture to 20 % or more resulted in a significant variation in the coating structure (fig. 4). The main difference from the previously considered coatings is the change in the type of formed eutectic from lamellar to skeleton. The structure of these coatings was also represented by primary borides with eutectic areas between it. It should be noted that chemical etching does not reveal the interphase boundaries between primary borides and eutectic colonies. Thus, the eutectic coalesced with the primary borides, which is clearly seen in Fig. 4b.

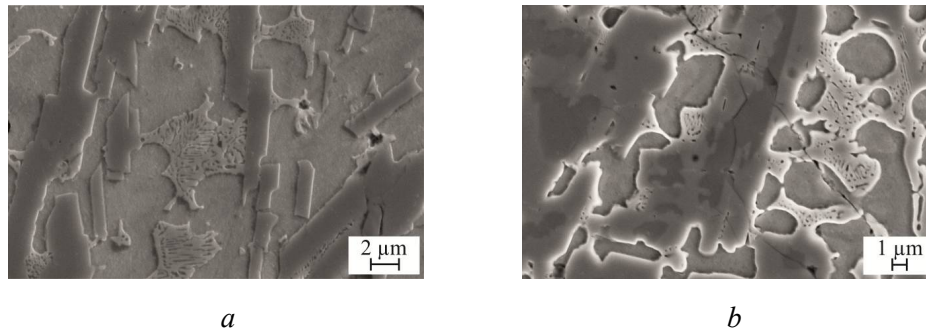


Fig. 4. Microstructure of borides in the coatings obtained by surfacing the powder mixtures with different *CrB* content:
a – 20 % *CrB*; *b* – 30 % *CrB*

The aforementioned change in the morphology of eutectic borides is presumably associated with a change in its composition and the type of crystal lattice. Table 3 shows the results of the elemental analysis of eutectic borides. It can be seen that in the coatings obtained from mixtures with the appending of 5 % and 10 % *CrB*, the main element in the composition of the borides is chromium (Table 3 and fig. 3). An increase in the fraction of borides in the surfacing mixture over 10 % led to a change in the elemental composition of eutectic borides. *Ni* was its main constituent element, while the chromium content decreased to 3–4 % (Table 3, fig. 5). These changes in the elemental composition led to a change in the type of crystal lattice, which will be discussed later along with results of X-ray diffraction analysis.

In addition, darker areas were found in the central part of the primary borides formed in the coating obtained by cladding the mixture with 30 % *CrB* (fig. 4b). Elemental analysis (fig. 5) revealed that in such areas, the chromium concentration is highest, while the mass fraction of other metals does not exceed 3 %. Thus, these regions presumably correspond to *CrB* borides. Crystals of primary borides formed around it contained manganese and iron, in addition to chromium.

The elemental analysis of the surfaced layers revealed the formation of a transition zone with a thickness of 50–150 μm enriched with iron (compared to the main part of the coating) at the boundary with the base material (fig. 6). The structure of this zone was heterogeneous; in a layer with a thickness of up to 10 μm, which was formed directly above the boundary, borides were not found (fig. 6a, c). Above the mentioned layer, eutectic borides appeared in the structure, but the large primary borides were not formed. The transition layer should have a favorable effect on the complex of the mechanical properties of materials since it decreases the alteration of properties between the surfaced layer and the base material.

Table 3

Elemental composition of eutectic borides

Amount of <i>CrB</i> in the mixture, %	<i>B</i> , %	<i>Cr</i> , %	<i>Mn</i> , %	<i>Fe</i> , %	<i>Co</i> , %	<i>Ni</i> , %
5	6.4	24.1	18.5	12.3	19.7	19.0
10	7.2	43.6	15.3	10.2	12.1	11.6
20	4.6	3.4	26.2	5.2	27.0	33.7
30	4.9	3.7	22.2	12.6	24.3	32.3

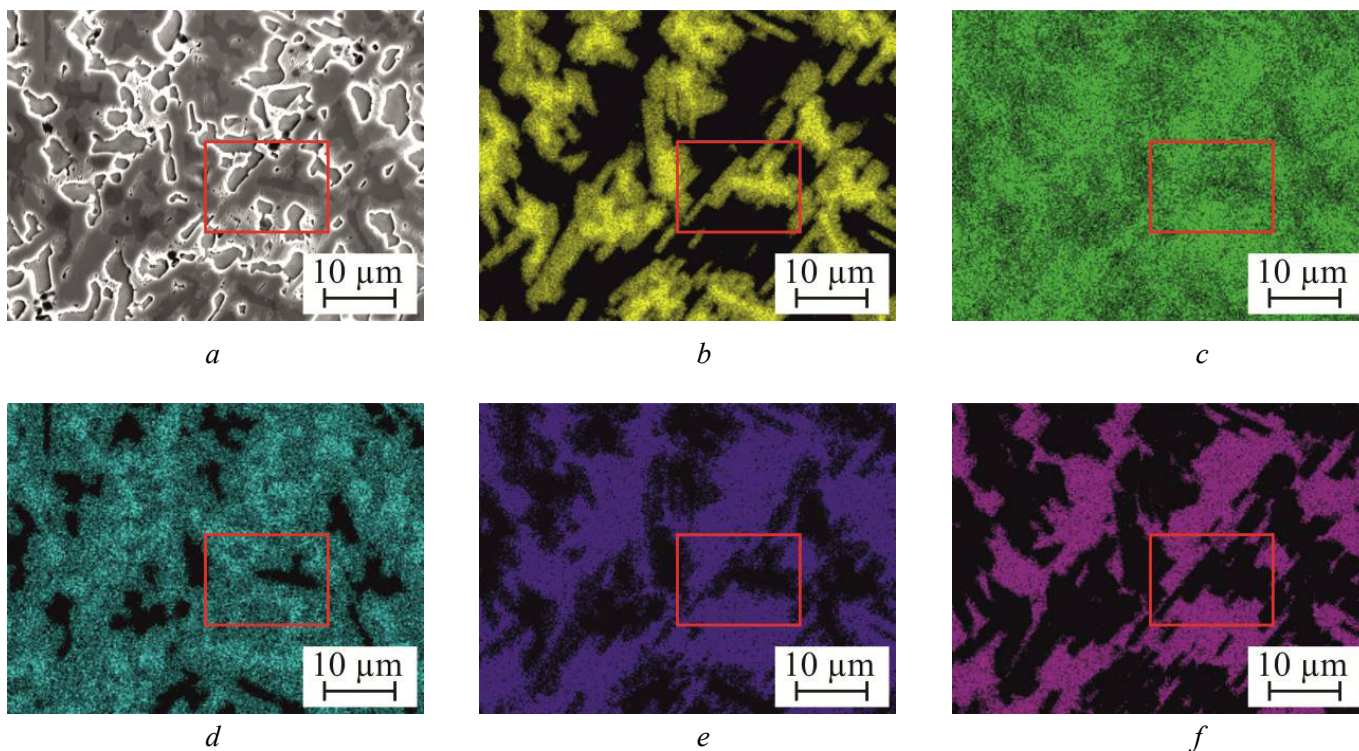


Fig. 5. Distribution of elements in the structure of the coating obtained by surfacing a powder mixture with 10 % CrB:

a – microstructure of the analyzed region; *b* – Cr; *c* – Mn; *d* – Fe; *e* – Co; *f* – Ni. The red square denotes the same analyzed region

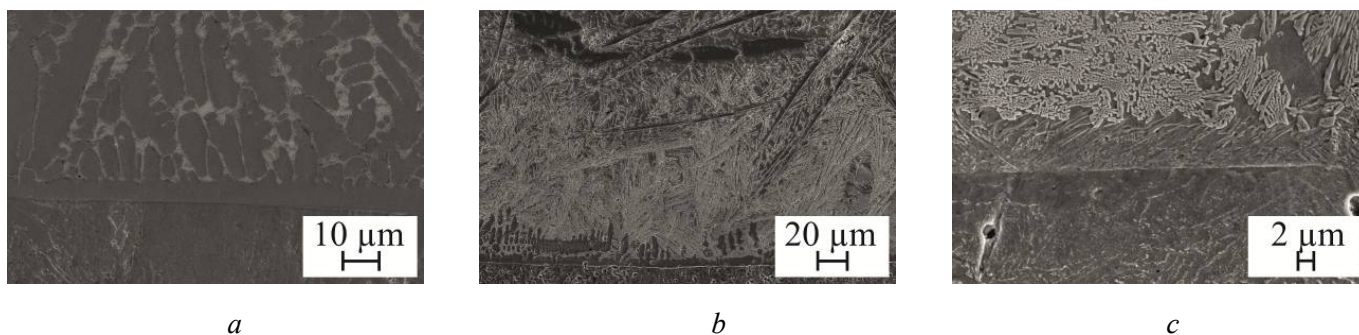


Fig. 6. Typical microstructure of the interfaces between a substrate and coatings obtained by surfacing the powder mixtures with different CrB content: CrB:

a – 5 % CrB; *b* – 10 % CrB; *c* – 30 % CrB

X-ray diffraction analysis of the surfaced layers

The diffraction patterns of the coatings obtained from powder mixtures with different CrB content are shown in fig. 7. The complexity of the analysis of the obtained patterns lies in the fact that a large number of borides or boride-based solid solutions belong to the same space symmetry groups and have close positions of diffraction maxima. Consequently, in fig. 7, only the space group is indicated without specifying the composition of the phase. In all samples, the formation of a solid solution with an *fcc* (*Fm-3m*) crystal lattice was observed. Specifically, the coating obtained without the addition of CrB particles had a single-phase structure. In samples with 5 % and 10 % CrB, weak reflections were found around 2θ of 31° , 56° , and 78° , which corresponds to a presence of a boride with an orthorhombic crystal lattice (*Fddd*). Cr_2B , Mn_2B , as well as solid solutions on its basis, namely $(Cr,Fe)_2B$ and $(Cr,Mn)_2B$, have such a lattice.

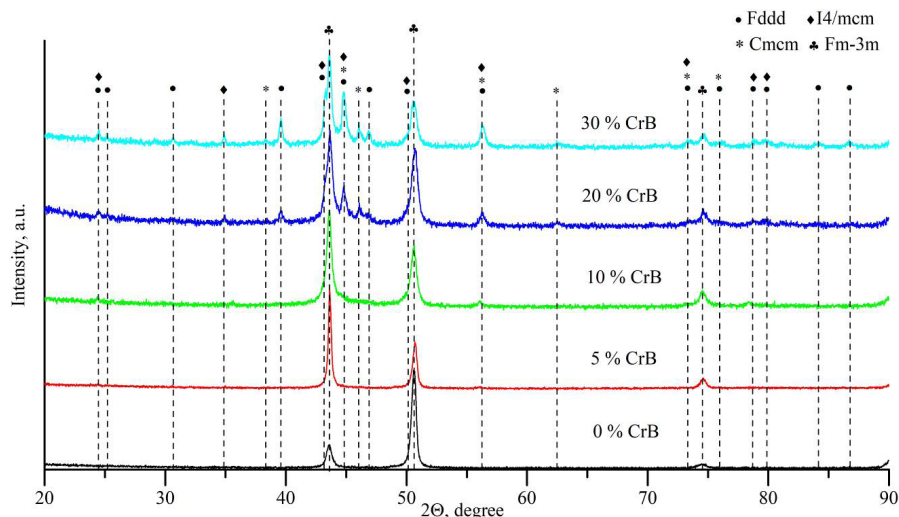


Fig. 7. X-ray diffraction patterns obtained by surfacing the powder mixtures with different CrB content

According to the results of the energy dispersive analysis and microstructural studies, it can be assumed that borides of the composition $(Cr,Mn,Fe)_2B$ were formed in the coatings under investigation.

An increase in the chromium boride amount in the surfacing mixture to 20 % and 30 % led to the appearance of reflections from borides with orthorhombic ($Cmcm$) and tetragonal ($I4/mcm$) crystal lattices in the diffraction patterns.

In the system under consideration, CrB , FeB , and MnB are borides with a lattice related to the $Cmcm$ space group. As mentioned above, in the sample obtained by surfacing the mixture with 30 % CrB , regions with composition close to the original boride that substantially did not contain other elements were observed. Thus, it can be assumed that the reflections from the phase that belongs to the $Cmcm$ space group correspond to CrB borides crystallized from the melt or original borides undissolved during surfacing.

Such borides as Mn_2B , Co_2B , Ni_2B , and Fe_2B belong to the $I4/mcm$ space group. Previously, it was shown that the structure of coatings with more than 20 % CrB usually exhibits the skeleton morphology of eutectic instead of lamellar. At the same time, in the skeleton eutectic, the concentration of Cr and Fe is much lower than that of Co , Mn , and Ni . The results obtained allow us to conclude that the boride found in the eutectic is a $(Ni,Co,Mn)_2B$ solid solution based on chemical compound.

On the basis of the conducted studies, one can assume the following scheme for the formation of the phase composition of coatings obtained by surfacing powder mixtures with different CrB content.

At a CrB concentration of 5 % (a hypoeutectic structure is formed):

- crystallization of the melt bath starts with the formation of dendrites based on fcc solid solution;
- increasing the concentration of boron in the melt brings its composition closer to the eutectic;
- in the interdendritic space, the eutectic consisting of $(Cr,Mn,Fe)_2B$ and the fcc phase crystallizes.

At a CrB concentration of 10 % (a hypereutectic structure is formed):

- primary borides $(Cr,Mn,Fe)_2B$ precipitate;
- the eutectic consisting of $(Cr,Mn,Fe)_2B$ and the fcc phase solidifies.

At CrB concentrations of 20 and 30 %:

- primary precipitation of CrB crystals with a higher melting point than that of Cr_2B phase from the melt bath occurs;
- $(Cr,Mn,Fe)_2B$ phase around CrB crystals forms;
- the eutectic consisting of $(Ni,Co,Mn)_2B$ and fcc solid solution crystallizes.

It is assumed that the change in the type of eutectic from the $(Cr,Mn,Fe)_2B + fcc$ phase to the $(Ni,Co,Mn)_2B + fcc$ phase is due to a decrease in the chromium content in the melt as a result of the primary precipitation of chromium-rich phases, such as CrB and $(Cr,Mn,Fe)_2B$.

Results of microhardness measurements of the fabricated materials

The evaluation of the mechanical properties of the coatings was carried out by measuring the microhardness according to the *Vickers* method. Fig. 8 shows the mean microhardness values of the surfaced layers. The average microhardness of the coating obtained without the *CrB* powder appending was $192 \pm 5 \text{ HV}_{0.1}$, which corresponds to the base material hardness. The addition of 5 % *CrB* led to an increase in hardness to $263 \pm 15 \text{ HV}_{0.1}$. An increase in the amount of *CrB* powder in the surfacing mixture to 10 %, 20 %, and 30 % led to an increase in the average microhardness values to $543 \pm 59 \text{ HV}_{0.1}$, $762 \pm 43 \text{ HV}_{0.1}$, and $1,141 \pm 91 \text{ HV}_{0.1}$, respectively. A significant increase in hardness is due to the formation of large amount of borides of various compositions and morphologies in the material structure.

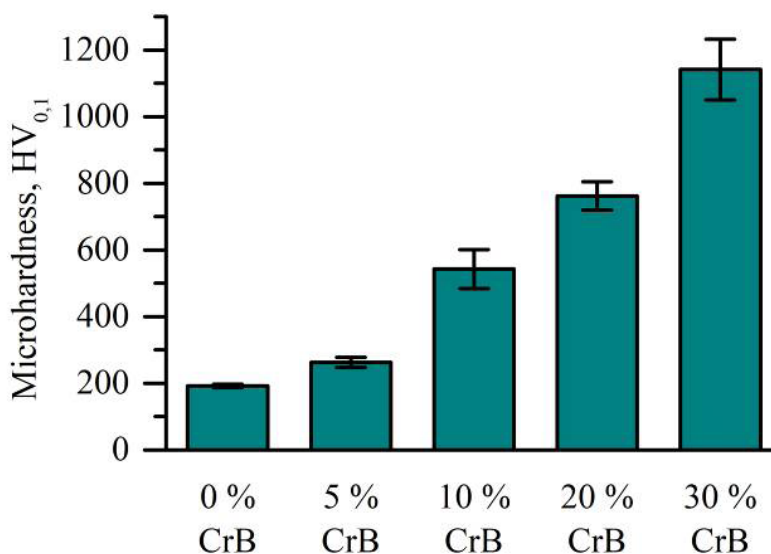


Fig. 8. Average microhardness of the coatings

Wear resistance of the coatings

The aforementioned changes in the structure and hardness of the coatings should affect its tribological characteristics. Fig. 9 shows typical diagrams that illustrate the dependence of coefficient of friction on the duration of the test. At the initial stage of testing, a wear-in process is observed accompanied by a gradual increase in the coefficient of friction. After the wear-in stage, the values of the friction coefficient stabilize.

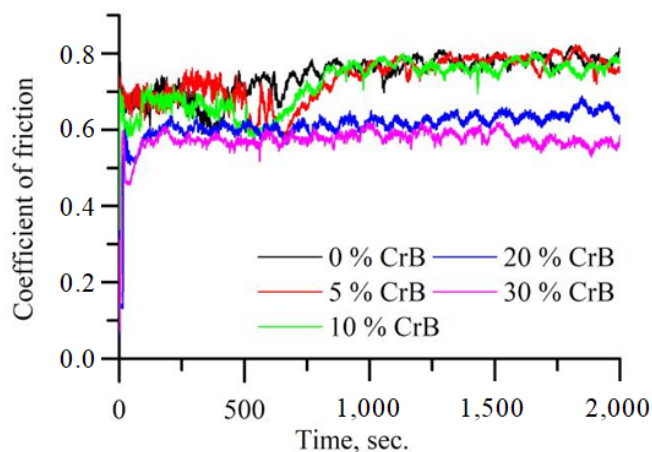


Fig. 9. Graphical representation of the change in the value of the friction coefficient during testing

It has been established that the structure of the coatings affects the duration of the wear-in process. In materials obtained by surfacing a mixture containing up to 10 % *CrB*, the duration of this stage is about 800 s. Increasing the content of *CrB* in the surfacing mixture to 20 % and 30 % leads to a 4-fold reduction in wear-in time.

The average values of the coefficient of friction are shown in Table 4. It was found that appending of 5 % and 10 % *CrB* into the powder mixture did not affect significantly the value of the friction coefficient. At the same time, the appending of 20 % and 30 % *CrB* promoted the reduction of the coefficient of friction from 0.71 to 0.62 and 0.57, respectively.

The wear resistance of the surfaced layers was evaluated by the volume of the wear crater (Table 4). The volume of the worn material of the coatings obtained by adding 5 % and 10 % *CrB* to the surfacing mixture was greater than that of the reference material. An increase in the amount of *CrB* particles to 20 % and 30 % favorably affected the wear resistance of the materials under investigation. It has been established that the volume of the worn material of the coatings obtained by surfacing the mixtures with 20 % and 30 % *CrB* was $0.17 \pm 0.04 \text{ mm}^3$ and $0.1 \pm 0.04 \text{ mm}^3$, respectively, which was 3 and 6 times lower than the value obtained for the specimen without *CrB* appending ($0.61 \pm 0.1 \text{ mm}^3$).

Table 4

Average values of the friction coefficients and the worn material volumes

No.	Composition	Friction coefficient	Average value of worn material, mm ³
1	<i>CoCrFeNiMn</i>	0.71 ± 0.22	0.61 ± 0.1
2	<i>CoCrFeNiMn</i> : <i>CrB</i> 95:5	0.73 ± 0.23	1.1 ± 0.09
3	<i>CoCrFeNiMn</i> : <i>CrB</i> 90:10	0.68 ± 0.22	0.77 ± 0.08
4	<i>CoCrFeNiMn</i> : <i>CrB</i> 80:20	0.62 ± 0.17	0.17 ± 0.04
5	<i>CoCrFeNiMn</i> : <i>CrB</i> 70:30	0.57 ± 0.15	0.1 ± 0.04

The wear resistance characteristics obtained are associated with a change in the structural and phase state of the coatings formed by appending different amounts of hardening particles.

An analysis of the friction surface of the coating obtained without appending reinforcing particles revealed that during testing, the material was plastically displaced from the friction zone to the periphery (fig. 10a). A similar character of the wear crater structure was observed in coatings containing 5 and 10 % *CrB* (fig. 10b). An increase in the amount of borides to 20 %, accompanied by an increase in microhardness, contributed to a decrease in plastic deformation. As a result, the material displacement was not observed on the friction surface (fig. 10c). An additional factor that prevents severe plastic deformation of the coating material is assumed to be the formation of a skeleton eutectic. As mentioned above, this type of eutectic connects separate primary borides and forms a spatial network.

The study of friction surfaces by scanning electron microscopy revealed signs of the adhesive wear of the coatings. Traces of seizure, delamination, and fracture of the material were found on the surface of the coatings (fig. 10d, f). These features are the mostly noticeable on the surface of the coating without hardening particles.

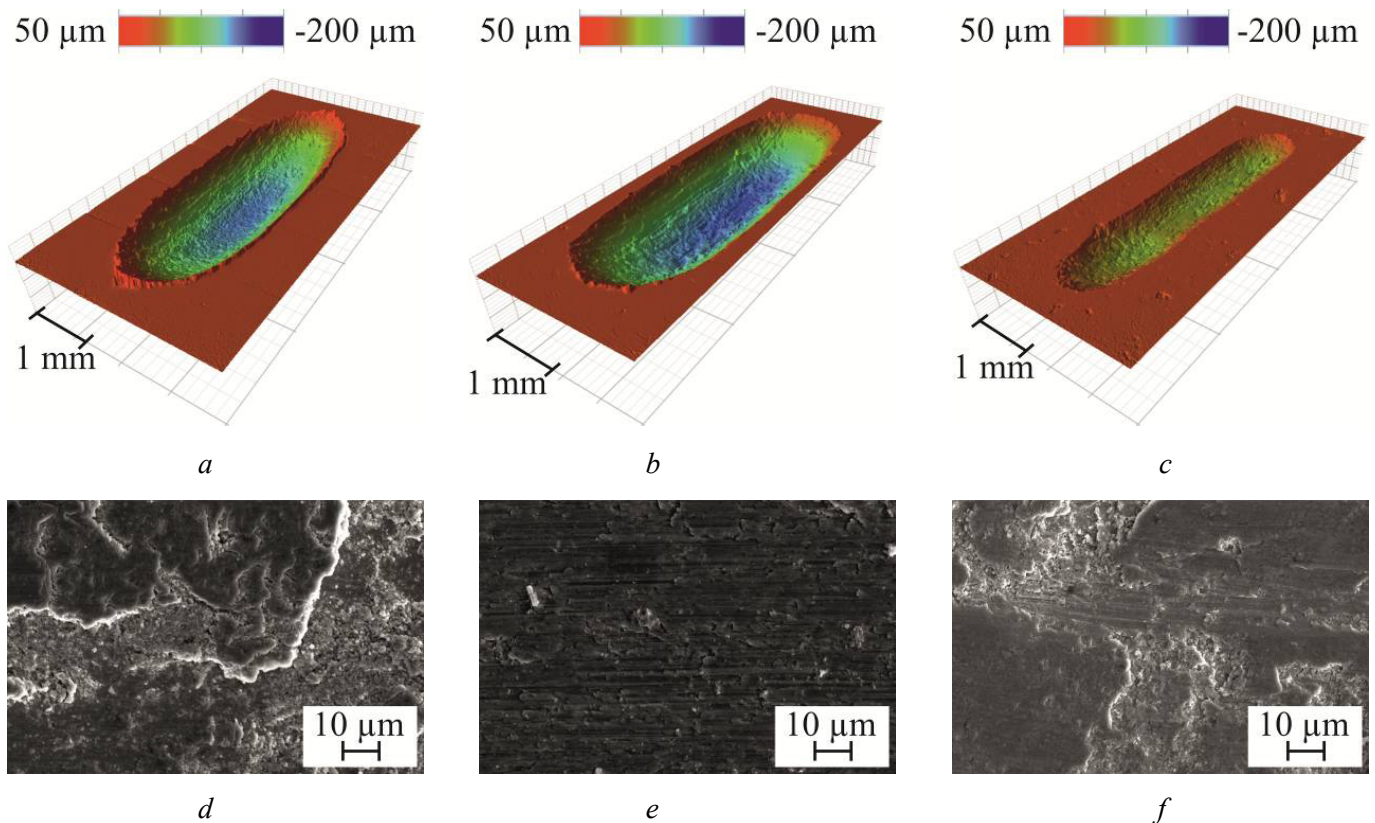


Fig. 10. Profiles of the wear grooves (a–c) and the wear surface micrographs (d–f);
 a – 0 % *CrB*; d – 0 % *CrB*; b – 10 % *CrB*; c – 20 % *CrB*; e – 5 % *CrB*; f – 30 % *CrB*



The addition of 5 % and 10 % CrB resulted in an increase in the volume of worn material despite an increase in the average microhardness of the coatings. Probably, the decrease in the wear resistance is associated with the formation of lamellar eutectic. During testing, the lamellar eutectic was degraded. The fracture products located in the contact zone between the counterbody and the specimen induced abrasive wear of the coating material (fig. 10e). With a higher content of chromium boride in the composition of the coatings, the proportion of the plastic matrix decreases, and the average microhardness of the coatings increases. As a result, the abrasive wear mechanism appears to a lesser extent.

Conclusions

With reference to the conducted research, it was established that regardless of the amount of CrB powder added to the surfacing mixture, a metal matrix based on the *fcc* solid solution was formed in the coatings. The appending of 5 % and 10 % CrB led to the formation of a lamellar eutectic consisting of $(Cr,Mn,Fe)_2B$ crystals and the *fcc* solid solution. An increase in the amount of CrB in the surfacing mixture to 20 % or more resulted in the formation of a metal matrix depleted in chromium, primary CrB-type borides, as well as a skeleton eutectic consisting of $(Ni,Co,Mn)_2B$ and the *fcc* solid solution in the structure.

An increase in the CrB fraction in the powder mixture from 0 to 30 % contributed to an increase in the average microhardness of coatings from 192 to 1,141 HV_{0.1}. Wear resistance testing of the coatings under investigation according to the ball-on-flat scheme revealed an adhesive wear mechanism. The appending 5 % and 10 % CrB led to additional abrasive wear by particles of eutectic borides and, accordingly, to a decrease in the wear resistance of coatings. Increasing the CrB content in the surfacing mixture to 20 % and 30 % contributed to an increase in the wear resistance of coatings by a factor of 3 and 6 compared to a material without CrB additions. Thus, the amount of worn material was reduced from 0.61 mm³ (0 % CrB) to 0.17 mm³ (20 % CrB) and 0.1 mm³ (30 % CrB), respectively.

References

1. Yeh J.W., Chen S.K., Lin S.J., Gan J.Y., Chin T.S., Shun T.T., Tsau C.H., Chang S.Y. Nanostructured high-entropy alloys with multiple principal elements: novel alloy design concepts and outcomes. *Advanced Engineering Materials*, 2004, vol. 6, iss. 5, pp. 299–303. DOI: 10.1002/adem.200300567.
2. Cantor B., Chang I.T.H., Knight P., Vincent A.J.B. Microstructural development in equiatomic multicomponent alloys. *Materials Science and Engineering: A*, 2004, vol. 375–377, pp. 213–218. DOI: 10.1016/j.msea.2003.10.257.
3. Tsai M.H., Yeh J.W. High-entropy alloys: a critical review. *Materials Research Letters*, 2014, vol. 2, iss. 3, pp. 107–123. DOI: 10.1080/21663831.2014.912690.
4. George E.P., Raabe D., Ritchie R.O. High-entropy alloys. *Nature Reviews Materials*, 2019, vol. 4, iss. 8, pp. 515–534. DOI: 10.1038/s41578-019-0121-4.
5. Steurer W. Single-phase high-entropy alloys – A critical update. *Materials Characterization*, 2020, vol. 162, pp. 1–17. DOI: 10.1016/j.matchar.2020.110179.
6. Zhang Y., Zuo T.T., Tang Z., Gao M.C., Dahmen K.A., Liaw P.K., Lu Z.P. Microstructures and properties of high-entropy alloys. *Progress in Materials Science*, 2014, vol. 61, pp. 1–93. DOI: 10.1016/j.pmatsci.2013.10.001.
7. Duchaniya R.K., Pandel U., Rao P. Coatings based on high entropy alloys: An overview. *Materials Today: Proceedings*, 2021, vol. 44, pp. 4467–4473. DOI: 10.1016/j.matpr.2020.10.720.
8. Li W., Liu P., Liaw P.K. Microstructures and properties of high-entropy alloy films and coatings: a review. *Materials Research Letters*, 2018, vol. 6, iss. 4, pp. 199–229. DOI: 10.1080/21663831.2018.1434248.
9. Jiang P.F., Zhang C.H., Zhang S., Zhang J.B., Chen J., Liu Y. Fabrication and wear behavior of TiC reinforced FeCoCrAlCu-based high entropy alloy coatings by laser surface alloying. *Materials Chemistry and Physics*, 2020, vol. 255, pp. 1–10. DOI: 10.1016/j.matchemphys.2020.123571.
10. Guo Y., Li C., Zeng M., Wang J., Deng P., Wang Y. In-situ TiC reinforced CoCrCuFeNiSi0.2 high-entropy alloy coatings designed for enhanced wear performance by laser cladding. *Materials Chemistry and Physics*, 2020, vol. 242, pp. 1–9. DOI: 10.1016/j.matchemphys.2019.122522.
11. Gu Z., Xi S., Sun C. Microstructure and properties of laser cladding and CoCr2.5FeNi2Tix high-entropy alloy composite coatings. *Journal of Alloys and Compounds*, 2020, vol. 819, pp. 1–10. DOI: 10.1016/j.jallcom.2019.152986.



12. Cheng J.B., Liang X.B., Wang Z.H., Xu B.S. Formation and mechanical properties of CoNiCuFeCr high-entropy alloys coatings prepared by plasma transferred arc cladding process. *Plasma Chemistry and Plasma Processing*, 2013, vol. 33, iss. 5, pp. 979–992. DOI: 10.1007/s11090-013-9469-1.
13. Hsu W.L., Murakami H., Yeh J.W., Yeh A.C., Shimoda K. On the study of thermal-sprayed $\text{Ni}_{0.2}\text{Co}_{0.6}\text{Fe}_{0.2}\text{CrSi}_{0.2}\text{AlTi}_{0.2}$ HEA overlay coating. *Surface and Coatings Technology*, 2017, vol. 316, pp. 71–74. DOI: 10.1016/j.surfcoat.2017.02.073.
14. Fadeev S.N., Golkovski M.G., Korchagin A.I., Kuksanov N.K., Lavruhin A.V., Petrov S.E., Salimov R.A., Vaisman A.F. Technological applications of BINP industrial electron accelerators with focused beam extracted into atmosphere. *Radiation Physics and Chemistry*, 2000, vol. 57, iss. 3–6, pp. 653–655. DOI: 10.1016/S0969-806X(99)00499-5.
15. Uvarov N.F., Bushueva E., Turlo Y., Khamgushkeeva G. Influence of chromium concentration on corrosion resistance of surface layers of stainless steel. *MATEC Web of Conferences*, 2021, vol. 340, pp. 1–5. DOI: 10.1051/mateconf/202134001022.
16. Bushueva E.G., Grinberg B.E., Bataev V.A., Drobyaz E.A. Raising the resistance of chromium-nickel steel to hydroabrasive wear by non-vacuum electron-beam cladding with boron. *Metal Science and Heat Treatment*, 2019, vol. 60, iss. 9–10, pp. 641–644. DOI: 10.1007/s11041-019-00331-3.
17. Lenitseva O.G., Bataev I.A., Golkovskii M.G., Bataev A.A., Samoilenko V.V., Plotnikova N.V. Structure and properties of titanium surface layers after electron beam alloying with powder mixtures containing carbon. *Applied Surface Science*, 2015, vol. 355, pp. 320–326. DOI: 10.1016/j.apsusc.2015.07.043.
18. Bataev I.A., Bataev A.A., Golkovski M.G., Krivizhenko D.S., Losinskaya A.A., Lenitseva O.G. Structure of surface layers produced by non-vacuum electron beam boriding. *Applied Surface Science*, 2013, vol. 284, pp. 472–481. DOI: 10.1016/j.apsusc.2013.07.121.
19. Bataev I.A., Golkovskii M.G., Losinskaya A.A., Bataev A.A., Popelyukh A.I., Hassel T., Golovin D.D. Non-vacuum electron-beam carburizing and surface hardening of mild steel. *Applied Surface Science*, 2014, vol. 322, pp. 6–14. DOI: 10.1016/j.apsusc.2014.09.137.
20. Lazurenko D.V., Alferova G.I., Golkovsky M.G., Emurlaev K.I., Emurlaeva Y.Y., Bataev I.A., Ogneva T.S., Ruktuev A.A., Stepanova N.V., Bataev A.A. Formation of wear-resistant copper-bearing layers on the surfaces of steel substrates by non-vacuum electron beam acladding using powder mixtures. *Surface and Coatings Technology*, 2020, vol. 395, p. 1–14. DOI: 10.1016/j.surfcoat.2020.125927.
21. Cantor B. Multicomponent high-entropy Cantor alloys. *Progress in Materials Science*, 2021, vol. 120, pp. 1–36. DOI: 10.1016/j.pmatsci.2020.100754.
22. Mridha S., Das S., Aouadi S., Mukherjee S., Mishra R.S. Nanomechanical behavior of CoCrFeMnNi high-entropy alloy. *JOM Journal of the Minerals Metals and Materials Society*, 2015, vol. 67, iss. 10, pp. 2296–2302. DOI: 10.1007/s11837-015-1566-6.
23. Zaddach A.J., Niu C., Koch C.C., Irving D.L. Mechanical properties and stacking fault energies of NiFeCrCoMn high-entropy alloy. *JOM Journal of the Minerals Metals and Materials Society*, 2013, vol. 65, iss. 12, pp. 1780–1789. DOI: 10.1007/s11837-013-0771-4.
24. Han Z., Ren W., Yang J., Tian A., Du Y., Liu G., Wei R., Zhang G., Chen Y. The corrosion behavior of ultra-fine grained CoNiFeCrMn high-entropy alloys. *Journal of Alloys and Compounds*, 2020, vol. 816, pp. 1–10. DOI: 10.1016/j.jallcom.2019.152583.
25. Laurent-Brocq M., Akhatova A., Perrière L., Chebini S., Sauvage X., Leroy E., Champion Y. Insights into the phase diagram of the CrMnFeCoNi high entropy alloy. *Acta Materialia*, 2015, vol. 88, pp. 355–365. DOI: 10.1016/j.actamat.2015.01.068.
26. Bataeva Z., Ruktuev A., Ivanov I., Yurgin A., Bataev I. Review of alloys developed using the entropy approach. *Metal Working and Material Science*, 2021, vol. 23, iss. 2, pp. 116–146. DOI: 10.17212/1994-6309-2021-23.2-116-146.
27. Zaddach A.J., Scattergood R.O., Koch C.C. Tensile properties of low-stacking fault energy high-entropy alloys. *Materials Science and Engineering: A*, 2015, vol. 636, pp. 373–378. DOI: 10.1016/j.msea.2015.03.109.
28. Gromov V.E., Rubannikova Y.A., Konovalov S.V., Osintsev K.A., Vorob'ev S.V. Generation of increased mechanical properties of Cantor hightentropy alloy. *Izvestiya vysshikh uchebnykh zavedenii. Chernaya Metallurgiya = Izvestiya. Ferrous Metallurgy*, 2021, vol. 64 (8), pp. 599–605. DOI: 10.17073/0368-0797-2021-8-599-605. (In Russian).
29. Zhang T., Zhao R.D., Wu F.F., Lin S.B., Jiang S.S., Huang Y.J., Chen S.H., Eckert J. Transformation-enhanced strength and ductility in a FeCoCrNiMn dual phase high-entropy alloy. *Materials Science and Engineering: A*, 2020, vol. 780, pp. 1–7. DOI: 10.1016/j.msea.2020.139182.
30. Uporov S.A., Ryltsev R.E., Bykov V.A., Estemirova S.K., Zamyatin D.A. Microstructure, phase formation and physical properties of AlCoCrFeNiMn high-entropy alloy. *Journal of Alloys and Compounds*, 2020, vol. 820, pp. 1–8. DOI: 10.1016/j.jallcom.2019.153228.



31. Fang S., Wang C., Li C.L., Luan J.H., Jiao Z.B., Liu C.T., Hsueh C.H. Microstructures and mechanical properties of CoCrFeMnNiV high entropy alloy films. *Journal of Alloys and Compounds*, 2020, vol. 820, pp. 1–8. DOI: 10.1016/j.jallcom.2019.153388.

32. Yim D., Sathiyamoorthi P., Hong S.J., Kim H.S. Fabrication and mechanical properties of TiC reinforced CoCrFeMnNi high-entropy alloy composite by water atomization and spark plasma sintering. *Journal of Alloys and Compounds*, 2019, vol. 781, pp. 389–396. DOI: 10.1016/j.jallcom.2018.12.119.

33. Shen L., Zhao Y., Li Y., Wu H., Zhu H., Xie Z. Synergistic strengthening of FeCrNiCo high entropy alloys via micro-TiC and nano-SiC particles. *Materials Today Communications*, 2021, vol. 26, pp. 1–7. DOI: 10.1016/j.mtcomm.2020.101729.

34. Hussain S.W., Mehmood M.A., Karim M.R.A., Godfrey A., Yaqoob K. Microstructural evolution and mechanical characterization of a WC-reinforced CoCrFeNi HEA matrix composite. *Scientific Reports*, 2022, vol. 12, iss. 1, p. 9822. DOI: 10.1038/s41598-022-13649-5.

35. Zhang B., Yu Y., Zhu S., Zhang Z., Tao X., Wang Z., Lu B. Microstructure and wear properties of TiN–Al₂O₃–Cr₂B multiphase ceramics in-situ reinforced CoCrFeMnNi high-entropy alloy coating. *Materials Chemistry and Physics*, 2022, vol. 276, p. 125352. DOI: 10.1016/j.matchemphys.2021.125352.

36. Mehmood M.A., Mujahid M., Godfrey A., Zafar M.F., Yaqoob K. Development and characterization of boride-reinforced CoCrFeNi composites. *Journal of Alloys and Compounds*, 2023, vol. 947, p. 169535. DOI: 10.1016/j.jallcom.2023.169535.

37. Chen X., Qin G., Gao X., Chen R., Song Q., Cui H. Strengthening CoCrFeNi high-entropy alloy by Laves and boride phases. *China Foundry*, 2022, vol. 19, iss. 6, pp. 457–463. DOI: 10.1007/s41230-022-1007-4.

38. Ruktuev A.A., Lazurenko D.V., Ogneva T.S., Kuzmin R.I., Golkovski M.G., Bataev I.A. Structure and oxidation behavior of CoCrFeNiX (where X is Al, Cu, or Mn) coatings obtained by electron beam cladding in air atmosphere. *Surface and Coatings Technology*, 2022, vol. 448, p. 128921. DOI: 10.1016/j.surfcoat.2022.128921.

Conflicts of Interest

The authors declare no conflict of interest.

© 2023 The Authors. Published by Novosibirsk State Technical University. This is an open access article under the CC BY license (<http://creativecommons.org/licenses/by/4.0>).

